



Adsorption of 2,4-dichlorophenol from aqueous solution by activated carbon derived from moso bamboo processing waste

Guang-qian Wu^{a,*}, Xin-yuan Sun^b, Hui Hui^c, Xin Zhang^d, Jie Yan^a, Qi-sheng Zhang^a

^aCollege of Wood Science and Technology, Nanjing Forestry University, Nanjing 210037, China
Tel. +86 25 85427133; Fax: +86 25 85427061; email: kdwu@163.com

^bTechnology Research Center, Nanjing CEC Environmental Protection Co., Ltd, Nanjing 211102, China

^cCollege of Environment, Hohai University, Nanjing 210098, China

^dSchool of Environment Science and Engineering, Donghua University, Shanghai 201620, China

Received 8 October 2012; Accepted 13 November 2012

ABSTRACT

The surface physical and chemical properties of activated carbon derived from moso bamboo processing waste (ACMB) were investigated using scanning electron microscopy, N₂ adsorption/desorption isotherm, Fourier transform infrared spectroscopy, and X-ray photoelectron spectroscopy (XPS). The adsorption characteristics of 2,4-dichlorophenol(2,4-DCP) on ACMB were also evaluated from various perspectives. The ACMB with particle size of 10–16 mesh was found to be suitable for adsorbing 2,4-DCP, and the adsorption capacity decreased considerably with increasing solution pH. The adsorption of 2,4-DCP on ACMB was fast initially, and the adsorption equilibrium could be reached within 480 min. The kinetic data could be best described by the pseudo-second-order model. The equilibrium data followed Langmuir and R-P isothermal models more precisely. The column adsorption results showed that the ACMB had a long term and stable ability to purify 2,4-DCP-containing wastewater and the saturated ACMB could be regenerated easily by NaOH solution.

Keywords: Moso bamboo; Activated carbon; Adsorption; 2,4-Dichlorophenol

1. Introduction

Bamboo is a type of abundant and inexpensive natural resource in south China. There are 34 genera and 534 species of bamboo in China, with a total forest area of about 5.38 million hectares. Bamboo culms of about 1.43 billion, more than 80% of which are moso bamboo culms, can be harvested with a total yield of about 20 million tons annually. The total species, growing stock, and harvesting amount of moso bamboo in China all topped the world in the last decade. In recent

years, the moso bamboo processing industry has been developed rapidly in South China and has contributed a lot to the local economy. However, millions of tons of moso bamboo processing waste are also yielded and discarded in open place annually without further usage. Apart from posing challenges to solid waste management, it also generate problems related to environment and health during its degradation and leaching processes, and may also pollute the receiving water bodies. Consequently, it is urgent to develop practical technologies to utilize the tremendous amount of moso bamboo processing waste.

*Corresponding author.

Previous researches suggested that moso bamboo processing waste is a type of excellent raw material to produce activated carbon [1,2], and the activated carbon derived from moso bamboo processing waste (ACMB) has been proven to be an environmentally friendly, low cost, and renewable bioresource with highly porous structure and huge surface area [1,3]. In recent years, the applications of ACMB in removal of gaseous pollutants [2], heavy metals [3,4], or toxic chemicals in wastewater [5,6] have been widely reported in literature.

2,4-Dichlorophenol (2,4-DCP) is a colorless, crystalline solid having the empirical formula $C_6H_4Cl_2O$, a molecular weight of 163.0, and a density of 1.383 at 25 °C. 2,4-DCP is a type of weak acid with $pK_a=7.85$ and is used primarily as an intermediate in making insecticides, herbicides, preservatives, antiseptics, disinfectants, and other organic compounds. 2,4-DCP is usually classified as a type of highly corrosive chemical; its lengthy or repeated contact may result in hypotension, myocardial failure, pulmonary edema, neurological changes, liver and renal toxicity, methemoglobinemia, and hemolysis; and any exposure may cause eye, skin, mouth, and gastrointestinal injuries [7].

In consideration of the hazardous effects of 2,4-DCP on human health and aquatic lives, the discharge of 2,4-DCP-containing wastewater is facing increasingly stringent limit in China (the permissible limit for 2,4-DCP in surface water is 0.093 mg/L in Chinese National Standard GB 3838–2002) and Canada (the guideline value of 2,4-DCP in drinking water is 0.09 mg/L in Canadian Water Quality Guidelines for Drinking Water Quality), and increasing attention has been paid to the development of 2,4-DCP removal technologies. Numerous studies have found that 2,4-DCP can be adsorbed and easily removed by various adsorbents, different types of carbonaceous adsorbents, such as nutshell activated carbons (ACs) and activated carbon fibers (ACFs), have been used to adsorb 2,4-DCP and high removal efficiencies can always be obtained [8–10].

However, to the best of our knowledge, the adsorption of 2,4-DCP on ACMB had not been investigated in previous studies and it was against the background that this study sought to evaluate the adsorption characteristics of 2,4-DCP on ACMB under varying experimental conditions. The kinetic and equilibrium data was also processed using various theoretical models to evaluate this adsorption process. In addition, the key surface properties of ACMB, including the surface morphology, surface functional groups, specific surface area, and pore size distribution were also investigated to elucidate the adsorption mechanisms. The goal of this study was to obtain a clear and comprehensive understanding of the adsorption characteristics of 2,4-DCP on ACMB.

2. Methods

2.1. Materials

The ACMB was provided by Zhongzhu Carbon Industry Co., Ltd. (Zhejiang, China). Firstly, the ACMB was finely ground and sieved to different meshes (6–10, 10–16, 60–80, 100–200, and 200–220 mesh, respectively), after having been washed in copious amount of deionized water, the ACMB particles were dried in the sun to eliminate moisture and were stored in desiccators. 2,4-DCP (AR grade) was purchased from Sinopharm Chemical Reagent Co., Ltd. (Shanghai, China). The deionized water was produced by an Ultra-pure UV water system manufactured by Hi-tech Instruments Co., Ltd. (Shanghai, China). All of the other chemicals were of AR grade and were used without further purification.

2.2. Analytical methods

Concentration of 2,4-DCP was determined by an UV–vis spectrophotometer (TU-1810, P-General Instrument Co., Ltd., China) according to the method provided by the literature [8–10], which was based on the measurement of maximum absorbance at λ_{max} 286 nm. The calibration curve of 2,4-DCP was also determined using this method and the same UV–vis spectrophotometer (the correlation coefficient R^2 was 0.9992). The surface morphology of ACMB was observed using scanning electron microscopy (SEM, Quanta-200, FEI Company, USA). The surface area and porosity of ACMB were determined by N_2 adsorption at 77 K with surface area and porosimetry analyzer (ASAP 2020, Micromeritics Corp, USA).

The ACMB was also analyzed using FTIR Spectrometer (IR360, Thermo Nicolet Ltd., USA), and the spectra were recorded from 4000 to 400 cm^{-1} . The X-ray photoelectron spectroscopy (XPS) measurement was carried out with a PHI5000 VersaProbe system (ULVAC-PHI, Chigasaki, Japan). The other instruments used in this study were a BT100–2J peristaltic pump (Longer Precision Pump Co., Ltd., Baoding, China), an acid meter (PHS-3C, Kangyi Instruments Co., Ltd., Shanghai, China), and an incubator shaker (HZP-250, Jionghong Instruments Co., Ltd., Shanghai, China).

2.3. Batch adsorption experiments

The batch adsorption experiments were carried out in a series of 250 mL conical flasks where 0.1 g ACMB and 50 mL of 2,4-DCP solution (25–500 mg/L) were added. The pHs of 2,4-DCP solution were adjusted to

different values using diluted solutions of HCl (1 mol/L) and NaOH (1 mol/L). These conical flasks were shaken in the incubator shaker at a speed of 100 rpm and a temperature of 293 K. Water samples in conical flasks were then filtered rapidly through 0.45 μm membranes, and the filtrates were used immediately to determine the concentrations of 2,4-DCP.

The equilibrium amount of 2,4-DCP adsorbed on ACMB (q_e mg/g) and the 2,4-DCP removal efficiency (% Removal) were calculated using Eqs. (1) and (2), respectively:

$$q_e = \frac{V(C_0 - C_e)}{m} \quad (1)$$

$$\% \text{ Removal} = \frac{(C_0 - C_e)}{C_0} \times 100 \quad (2)$$

where C_0 and C_e (mg/L) are the initial and equilibrium concentrations of 2,4-DCP, respectively; V (L) is the volume of 2,4-DCP solution; and m (g) is the mass of ACMB.

To determine the best-fit model for the adsorption process, the nonlinear curve fitting facility of Microcal Origin 7.5 was employed to simulate and evaluate the fitting of the adsorption kinetic and isothermal models to the experimental data. To compare the validity of each model, a normalized standard deviation Δq_e (%) was calculated using Eq. (3):

$$\Delta q_e(\%) = 100 \sqrt{\frac{\sum_i^N [(q_{i,\text{exp}} - q_{i,\text{cal}})/q_{i,\text{exp}}]^2}{(N - 1)}} \quad (3)$$

where N is the total number of data points and i is the serial number of each data point; $q_{i,\text{exp}}$ (mg/g) and $q_{i,\text{cal}}$ (mg/g) are the experimental and calculated adsorption amount of 2,4-DCP at each data point.

2.4. Fixed-bed column runs

Column adsorption tests were carried out with a polyethylene column (30 mm internal diameter and 350 mm length) at 293 K, and 60 g of ACMB particles (6–10 mesh, the packing volume was 200 mL) were packed within this column uniformly. The absorbent cotton was used at the top and bottom of the column to disperse flow through the area and to prevent the escape of ACMB particles from the column. The feeding 2,4-DCP solution with concentration of 20 mg/L and pH of 7.0 was prepared and pumped up-flow through the column at a rate of four bed volumes per

hour (4 BV/h). The effluent was collected and the concentration of 2,4-DCP was determined, then the dynamic adsorption curve was plotted. The desorption experiment was performed using NaOH solution with concentration of 1.0 mol/L as eluting agent, and the flow rate of NaOH solution was controlled at 1 BV/h. The eluent was collected at varying intervals and the concentration of 2,4-DCP was determined, and then the desorption curve was plotted.

3. Results and discussion

3.1. Characterization of ACMB

The SEM image of ACMB was shown in Fig. 1. As could be seen in this figure, a well-developed cellular structure could be clearly found on the cross section of ACMB particle, this type of structure was quite different from those of other carbonaceous adsorbents, such as various nutshell ACs or ACFs. The sizes of these cells ranged from several to dozens of micrometers according to the scale on Fig. 1.

Numerous pores, including the micro-, meso-, and macropores, were distributed in the internal spaces of these cells and contributed most to the total surface area of ACMB. The unique cellular structure of ACMB originated from the intrinsic composition and distribution of the vascular bundles and parenchyma tissues of raw moso bamboo, which are the main constituents of the central cylinder of the internodes [11], the organic contents in these vascular bundles and parenchyma tissues could be decomposed and vaporized completely in the process of carbonization and subsequent activation, then the resulting cellular structure was yielded.

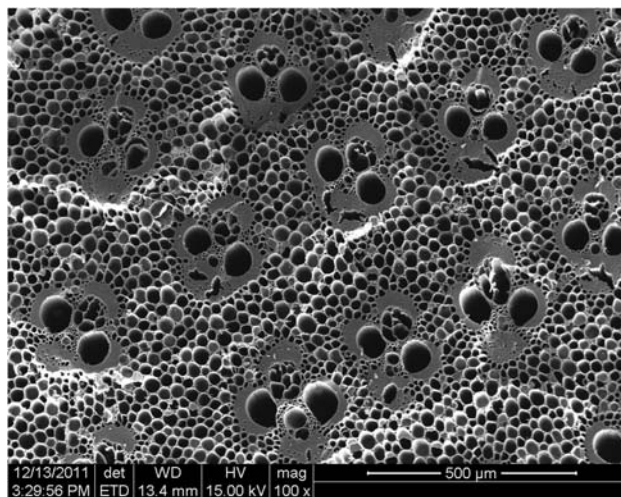


Fig. 1. Scanning electron microphotograph (SEM) of ACMB at 100x.

The N_2 adsorption/desorption curves and pore size distribution of ACMB were shown in Fig. 2, and the structural parameters of ACMB including the BET surface area, pore volume, and average pore width were summarized in Table 1.

The shape of this adsorption/desorption isotherm was a mixture of type I and IV isotherms in the IUPAC classification, with a quite narrow hysteresis loop at high relative pressure, and a vast majority of the pores of ACMB fell into the range between 2 and 10 nm, suggesting that a mixed microporous and mesoporous structure was dominant in the porosity of ACMB.

The FTIR analysis permitted spectrophotometric observation of the ACMB surface in the range 4000–400 cm^{-1} and served as a direct means for the identification of the surface functional groups. The FTIR spectrum of ACMB was shown in Fig. 3.

The broad absorption band at about 3430 cm^{-1} was assigned to the O–H stretching vibration of hydroxyl group, which was usually derived from the carboxylic groups, phenolic groups, and adsorbed H_2O molecules. The small absorption bands at 2920 and 2850 cm^{-1} were due to the symmetric and asymmetric C–H stretching vibration. The absorption band at about 1630 cm^{-1} could be assigned to the stretching vibration of aromatic C=C bond on the graphene layer of ACMB. The small absorption bands at about 1460 and 1380 cm^{-1} were associated with the asymmetric deforming vibration of –CH₃ and –CH₂. The broad band occurring at 1050 cm^{-1} was mainly related with the C–O stretching vibration of alcoholic, phenolic, and carboxylic groups. Another absorption band was found at 850 cm^{-1} , which was expected to be associated with the out-of-plane bending mode of O–H.

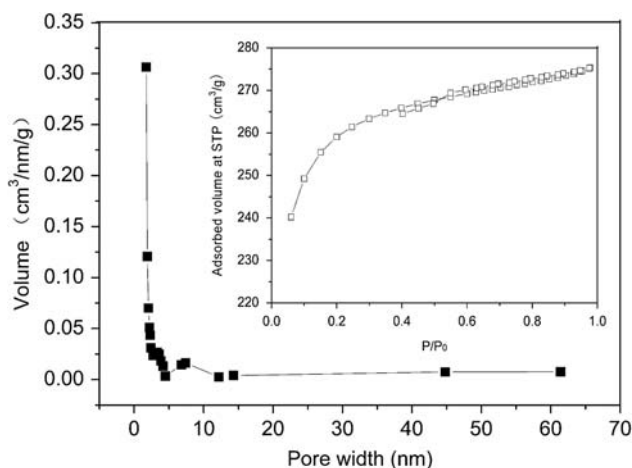


Fig. 2. N_2 adsorption/desorption curves and pore size distribution of ACMB.

The XPS survey spectra exhibited prominent peaks due to carbon, oxygen, and nitrogen [12]. In this study, the high-resolution spectra of C1s, N1s, and O1s were acquired over 278–298, 392–412, and 523–543 eV, with the same step size of 0.1 eV, the intensity of the XPS peak was recorded as counts per second (CPS), which was provided in Fig. 4. Table 1 summarized the elemental composition (at.%) of the ACMB over the sampling depth of several atomic layers from the surface. It was clear that the C atoms were predominant in the elemental composition, while the N atoms only accounted for a little portion of the elemental composition, and the O atoms were responsible for the remaining elemental composition besides C and N atoms. High-resolution XPS spectra of the C1s region were also presented in Fig. 4, which indicated several carbon species on the surface of ACMB. The optimum fitting was achieved by deconvolution of five peaks for each C1s spectrum: graphitic carbon (284.6 eV), carbon present in phenolic, alcohol, and ether groups (C–O, 285.5 eV), carbonyl groups (C=O, 287 eV), carboxyl, lactone, or ether groups (O=C–O, 288.6 eV), and shake-up satellite peaks due to π – π transitions in aromatic rings (290.2 eV). The relative content of each functional group was obtained from the corresponding area of small peaks divided by the total area, which was shown in Table 2.

3.2. Effect of particle size on adsorption of 2,4-DCP

The effect of particle size on adsorption of 2,4-DCP on ACMB was investigated, and five size ranges (6–10, 10–16, 60–80, 80–100, and 200–220 mesh) were used in this experiment.

The result was shown in Fig. 5, which showed that the removal efficiencies (% Removal) and equilibrium adsorption amount (q_e) increased gradually with the decrease in particle sizes; however, it was also notable that the increase in removal efficiencies was not directly proportional to the decrease in particle sizes, and the removal efficiency and q_e of ACMB with particle size of 10–16 mesh were nearly equal to those with particle sizes of 60–80, 80–100, and 200–220 mesh. Consequently, the further decrease in particle size was uneconomic and ineffective in practical application, and the particle size of 10–16 mesh was totally employed in the following experiments. The reason for this result could be explained as follows: the highly porous structure of ACMB made most of the active sites in the internal pores accessible to 2,4-DCP molecules despite the specific particle sizes of ACMB, so the amounts of active sites of ACMB could not increase sharply with the decrease in particle sizes.

Table 1
Characterization of ACMB

Surface area and porosity				Elemental composition				
S_{BET}	D_p (nm)	V_t (cm ³ /g)	V_m (cm ³ /g)	C (at.%)	O (at.%)	N (at.%)	O/C (at.%)	N/C (at.%)
791	2.286	0.452	0.289	89.43	9.59	0.98	10.72	1.09

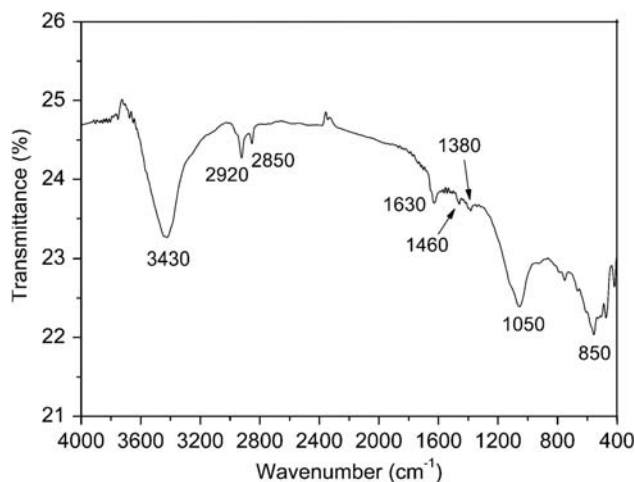


Fig. 3. The FTIR spectrum of ACMB.

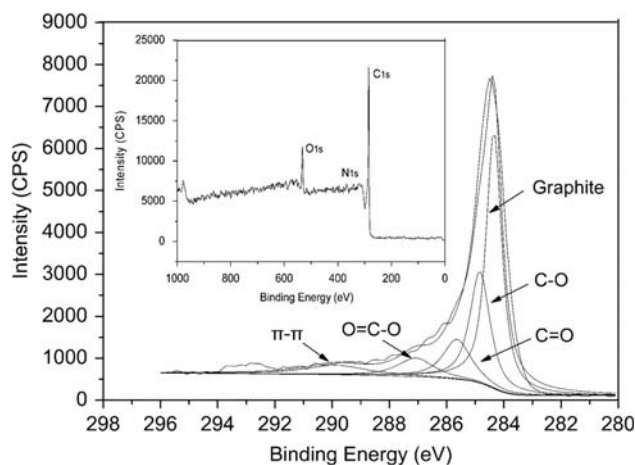


Fig. 4. The XPS spectrum of ACMB.

3.3. Effect of solution pH on adsorption of 2,4-DCP

The solution pH was one of the most significant parameters in the adsorption process. The solution pH primarily affected the degree of ionization of 2,4-DCP and the surface properties of ACMB. In this study, the effect of solution pH on adsorption of 2,4-DCP was investigated over the pH range of 1.0–13.0 with the initial concentration of 2,4-DCP fixed at 400 mg/L.

The result was shown in Fig. 6, which showed that the effluent concentration of 2,4-DCP increased with

the rise of solution pH. Similar observations have been reported for the adsorption of 2,4-DCP by cattail fiber-based activated carbon [13], agricultural waste-based activated carbon [14], and Mn-modified activated carbon prepared from *Polygonum orientale* Linn [9]. All of these researches demonstrated that lower solution pHs were favorable for the adsorption of 2,4-DCP on carbonaceous adsorbents.

The effect of solution pH on adsorption of 2,4-DCP could be explained as follows: the 2,4-DCP is a hydrophilic organic compound and could be present in solution in two forms—protonated and deprotonated species. Their percentages presented in solution are dependent on the solution pH, and more than 99% of all 2,4-DCP would be in the form of protonated species at pH < 6.0, whereas more than 95% of all 2,4-DCP would be in the form of deprotonated species [9,13].

In previous research [5], the pH_{pzc} value of ACMB had been carefully investigated, and the exact pH_{pzc} value of ACMB was taken as 8.71. The effects of pH_{pzc} value on the surface properties of ACMB were summarized in the literature [15–17]. When ACMB was introduced into an aqueous environment, their surface charges were positive if solution pH < pH_{pzc} and were negative if solution pH > pH_{pzc}; when solution pH was equal to the pH_{pzc} of ACMB, the surface of ACMB was electrically neutral.

At acidic pHs 1.0–7.0 (pHs < pK_a, pK_a of 2,4-DCP is 7.85), most of the 2,4-DCP molecules were in the nonionized forms, whereas the surface of ACMB was positively charged, in this case, no electrostatic repulsion occurred between the surface of ACMB and the 2,4-DCP molecules, consequently, higher adsorption capacities could be obtained. However, at basic pHs 9.0–13.0 (pHs > pK_a), the 2,4-DCP dissociated, forming dichlorophenate anions, whereas the surface of ACMB was also negatively charged. Thus, the electrostatic repulsion between dichlorophenate anions and the surface of ACMB interfered with the adsorption of 2,4-DCP considerably. On the other hand, at basic pHs, the adjacent dichlorophenate anions adsorbed on the surface of ACMB would repel each other to a significant degree, and this repulsion force would offset the Van der Waals force or the other adsorption forces [16,17]. Therefore, the adsorbed 2,4-DCP molecules

Table 2
The relative content of each carbon-containing functional groups measured by XPS

Functional groups	Electron binding energy (eV)	Relative intensity (%)
Graphite	284.6	46.7
C–O	285.5	26.0
C=O	287.0	12.8
O=C–O	288.6	7.7
π - π	290.2	6.8

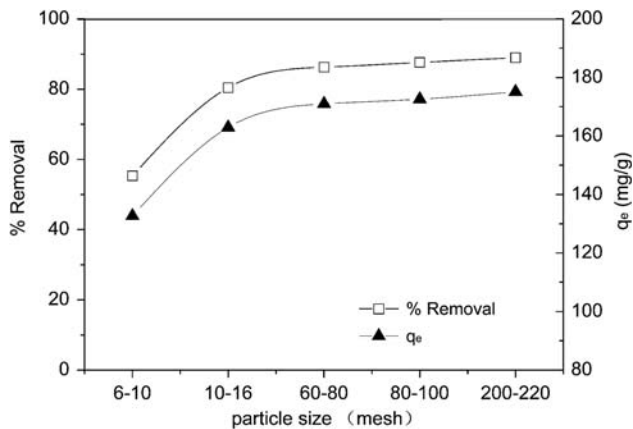


Fig. 5. Effect of particle size on adsorption of 2,4-DCP on ACMB. (Solution pH=7.0, $C_0=400$ mg/L, ACMB dosage = 0.1 g/50 mL, shaking time = 480 min, shaking speed = 100 rpm, and temperature = 293 K).

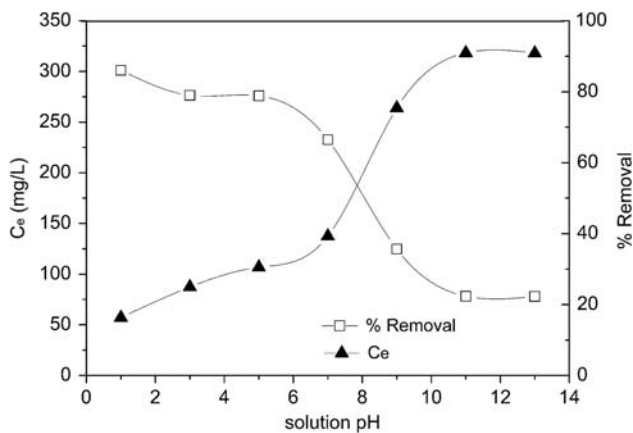


Fig. 6. Effect of solution pH on adsorption of 2,4-DCP on ACMB. (Solution pH=1.0–13.0, $C_0=400$ mg/L, ACMB dosage = 0.1 g/50 mL, shaking time = 480 min, shaking speed = 100 rpm, and temperature = 293 K).

could not pack together densely on the surface of ACMB, as a result, the equilibrium adsorption capacity decreased considerably.

3.4. Adsorption kinetics

The effect of contact time on adsorption of 2,4-DCP on ACMB was showed in Fig. 7. It could be found that the adsorption amounts of 2,4-DCP (q_t) increased gradually with the rise of contact time until q_t remained invariable. The equilibrium adsorption amounts of 2,4-DCP (q_e) was 165.7 mg/g with the initial 2,4-DCP concentration of 400 mg/L. The adsorption equilibrium of 2,4-DCP on ACMB could be reached within 480 min, and more than 70% of the equilibrium adsorption amounts could be obtained within the initial 120 min.

In order to investigate the adsorption processes of 2,4-DCP on ACMB, kinetic analyses were usually conducted using pseudo-first-order and pseudo-second-order models. The equation of pseudo-first-order model could be expressed as follows:

$$\lg(q_{e,cal} - q_t) = \lg q_{e,cal} - \frac{k_1 t}{2.303} \quad (4)$$

The equation of pseudo-second-order model could be expressed as follows:

$$\frac{t}{q_t} = \frac{1}{k_2 q_{e,cal}^2} + \frac{t}{q_{e,cal}} \quad (5)$$

where $q_{e,cal}$ (mg/g) is the calculated equilibrium amount of 2,4-DCP adsorbed on ACMB using these two models; q_t (mg/g) is the amount of 2,4-DCP adsorbed on ACMB at time t (min); k_1 (1/min) is the rate constant of pseudo-first-order model; and k_2 (g/(mg·min)) is the rate constant of pseudo-second-order model.

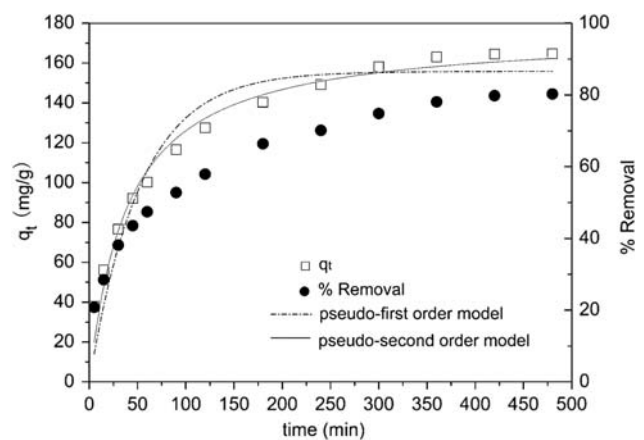


Fig. 7. The kinetic models for adsorption of 2,4-DCP on ACMB. (Solution pH=7.0, $C_0=400$ mg/L, ACMB dosage = 0.1 g/50 mL, shaking time=(5–480) min, shaking speed = 100 rpm, and temperature = 293 K).

The regression curves of pseudo-first-order and pseudo-second-order models were also shown in Fig. 7, the corresponding kinetic parameters were listed in Table 3.

As seen from Fig. 7, the pseudo-first-order model did not show a good agreement with the experimental kinetic data, which could also be concluded from the lower correlation coefficients ($R^2=0.9282$) and larger normalized standard deviation Δq_e (11.24%) listed in Table 3. However, the pseudo-second-order model fitted the experimental data well, and the correlation coefficients (R^2) and the normalized standard deviation (Δq_e) were 0.9760 and 5.63%, respectively. Furthermore, the values of q_e calculated by pseudo-second-order model ($q_{e,cal}=171.6$ mg/g) was in good agreement with the experimental value $q_{e,exp}$ ($q_{e,exp}=165.7$ mg/g). Therefore, the pseudo-second-order model was suitable to describe the adsorption of 2,4-DCP on ACMB.

3.5. Adsorption isotherms

The equilibrium data of adsorption process was shown in Fig. 8. It was obvious that the equilibrium adsorption amounts (q_e) increased with the rise of equilibrium concentrations (C_e) of 2,4-DCP. In this study, the equilibrium data was analyzed using Langmuir, Freundlich, Redlich–Peterson (R–P), and Temkin isothermal models.

The nonlinear form of Langmuir isothermal model was presented in Eq. (6):

$$q_e = \frac{C_e K_L q_{\max}}{1 + C_e K_L} \quad (6)$$

where q_e (mg/g) is the equilibrium adsorption amount of 2,4-DCP; C_e (mg/L) is the equilibrium concentration of 2,4-DCP; q_{\max} (mg/g) is the maximum monolayer adsorption amount of 2,4-DCP; and K_L (L/mg) is the Langmuir constant.

The Freundlich isothermal model is an empirical equation, and it could be written in a nonlinear form, which is presented in Eq. (7):

$$q_e = K_F C_e^{1/n} \quad (7)$$

where C_e (mg/L) is the equilibrium concentration of 2,4-DCP; K_F (mg/g (L/mg) $^{1/n}$) and n are Freundlich constants; n gives an indication of how favorable the adsorption is; and K_F is the adsorption capacity of ACMB.

The Redlich–Peterson (R–P) isothermal model incorporates the features of both the Langmuir and the Freundlich isothermal models. It considers, as the Freundlich model, heterogeneous adsorption surfaces as well as the possibility of multilayer adsorption. The R–P isothermal model is presented in Eq. (8):

$$q_e = \frac{a C_e}{1 + b C_e^n} \quad (8)$$

where a, b and n are the isothermal constants; q_e (mg/g) is the equilibrium adsorption amount of 2,4-DCP; and C_e (mg/L) is the equilibrium concentration of 2,4-DCP.

The linear form of Temkin isothermal model is presented in Eq. (9):

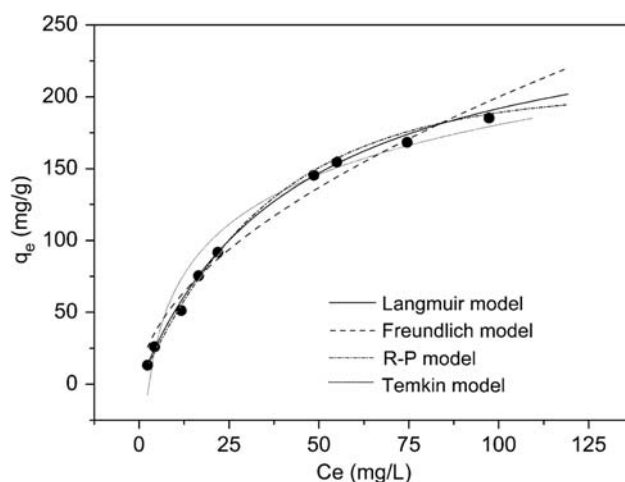


Fig. 8. The isothermal models for adsorption of 2,4-DCP on ACMB. (Solution pH = 7.0, $C_0 = (25\text{--}500)$ mg/L, ACMB dosage = 0.1 g/50 mL, shaking time = 480 min, shaking speed = 100 rpm, and temperature = 293 K).

Table 3
Kinetic parameters for adsorption of 2,4-DCP on ACMB

Pseudo-first-order model					Pseudo-second-order model				
$q_{e,exp}$ (mg/g)	$q_{e,cal}$ (mg/g)	k_1 (1/min)	R^2	Δq_e (%)	$q_{e,exp}$ (mg/g)	$q_{e,cal}$ (mg/g)	k_2 (g/(mg.min))	R^2	Δq_e (%)
165.7	147.8	0.043	0.9282	11.24	165.7	171.6	1.4×10^{-3}	0.9760	5.63

* $q_{e,exp}$ was the equilibrium amount of 2,4-DCP adsorbed on ACMB obtained in experiments.

Table 4
Isothermal parameters for the adsorption of 2,4-DCP on ACMB

<i>Langmuir isothermal model</i>	
q_{\max} (mg/g)	276.2
K_L (L/mg)	0.0228
R^2	0.9959
Δq_e (%)	6.05
<i>Freundlich isothermal model</i>	
n	1.85
K_F ((mg/g)(L/mg) ^{1/n})	16.556
R^2	0.9681
Δq_e (%)	10.49
<i>R–P isothermal model</i>	
a	5.276
b	0.00552
n	1.255
R^2	0.9979
Δq_e (%)	5.86
<i>Temkin isothermal model</i>	
k_t (L/mg)	0.37
b (J/mol)	47.70
B (L/g)	50.01
R^2	0.9544
Δq_e (%)	16.42

$$q_e = B \log k_t + B \log C_e \quad (9)$$

where $B = RT/b$ represents the heat of adsorption; T is the absolute temperature in Kelvin, and R is the universal gas constant; $1/b$ indicates the adsorption potential of the adsorbent while k_t (L/mg) is the equilibrium binding constant corresponding to the maximum binding energy.

The regression curves of four types of isothermal models are presented in Fig. 8, and all of the parameters obtained in these models are presented in Table 4.

It was clear that the equilibrium data could be best fitted by Langmuir (the correlation coefficients R^2 were 0.9959) and R–P isothermal model (the correlation coefficients R^2 were 0.9979), and the values of Δq_e of Langmuir and R–P models listed in Table 4 were quite smaller than those of Freundlich and Temkin models. The maximum monolayer adsorption capacity (q_{\max}) calculated by Langmuir isothermal model was 276.2 mg/g.

A great many of studies have investigated 2,4-DCP adsorption by various adsorbents, and the Langmuir isothermal model had been fully proven to be suitable to describe the adsorption equilibrium by these studies, the maximum monolayer adsorption capacities calculated by Langmuir isothermal model obtained by these studies are given in Table 5, and it was found that the ACMB could be classified as a type of highly efficient adsorbent for the removal of 2,4-DCP from aqueous solution.

Table 5
Comparison of adsorption capacities of 2,4-DCP with various adsorbents

Adsorbent	Maximum monolayer adsorption capacity (mg/g)	References
Ammonia-modified activated carbon	285.71 (30°C) 303.03 (40°C) 312.50 (50°C)	[8]
Activated carbon derived from agricultural waste	232.56 (30°C)	[14]
Static-air-activated carbon fiber	399 (25°C)	[16]
Cattail fiber-based activated carbon	142.86 (20°C) 135.14 (30°C) 133.33 (40°C)	[13]
Activated carbon derived from oil palm empty fruit bunches	27.25 (30°C)	[18]
Maize cob carbon	17.94 (25°C)	[10]
Activated carbon fiber	372 (20°C)	[17]
Organic bentonite	281.8 (30°C)	[19]
Carbon nanotube	30.53 (25°C)	[20]
Cationic sawdust cellulose	1.48 (25°C)	[21]
Cross-linked polyvinylimidazole microspheres	143(20°C)	[22]
ACMB	276.2(20°C)	Present work

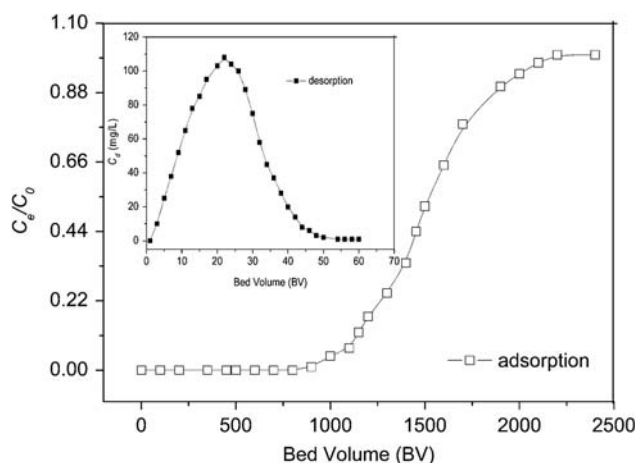


Fig. 9. Fixed-bed column adsorption and desorption curves. (Solution pH = 7.0, $C_0 = 20$ mg/L, 2,4-DCP influent flow rate = 4 BV/h, NaOH eluent flow rate = 1 BV/h, and temperature = 293 K).

3.6. Fixed-bed column adsorption and regeneration

Adsorption in continuous flow fixed-bed column is often preferred because it is simple to operate and can be scaled up readily. In this study, the 2,4-DCP in the column effluent was detected when the influent reached about 900 BV, and the ACMB column was saturated at about 2200 BV (Fig. 9).

The leaking and saturated adsorption amounts were calculated to be 61.5 and 123.2 mg/g, respectively, which were much little than the equilibrium adsorption amount obtained in the batch experiments (165.7 mg/g), and the much shorter contact time and insufficient mass transfer process should be responsible for this distinction. The desorption curve of 2,4-DCP from ACMB is also presented in Fig. 9. It could be seen that the shape of the desorption curve was cuspsate, and the desorbed 2,4-DCP in the NaOH eluent was detected at the beginning of the desorption process. The 2,4-DCP concentration in the NaOH eluent reached the peak value at about 22 BV ($C_d = 107.3$ mg/L) and the calculation results showed that 2,4-DCP could be eluted from ACMB column with a desorption ratio of 98.4% within 60 BV. This revealed fully that ACMB saturated by 2,4-DCP could be regenerated by NaOH eluent rapidly and easily reused.

4. Conclusions

This study investigated the surface physical and chemical properties of ACMB. The adsorption of 2,4-DCP on ACMB was also evaluated from various perspectives. The experimental results suggested that the

ACMB with particle size of 10–16 mesh was quite suitable to adsorb 2,4-DCP, and the adsorption capacity decreased with increasing solution pHs. The pseudo-second-order model could best describe the adsorption kinetics, and the equilibrium data fitted very well with Langmuir and R-P isothermal models. The fixed-bed column experiments showed the ACMB had a long term and stable ability to purify 2,4-DCP containing wastewater.

Acknowledgments

The authors would like to acknowledge financial support for this work provided by Project of the Priority Academic Program Development (PAPD) of Jiangsu Higher Education Institutions.

References

- [1] J.H. Fu, S.T. Yin, Utilization of bamboo charcoal, *World Bamboo Rattan* 7 (2009) 40–43.
- [2] Q.S. Chen, W.Y. Zhu, Study on Photocatalytic Degradation of Formaldehyde by TiO_2 Loaded on Bamboo Charcoal, *J. Fujian Normal Univ.* 25 (2009) 72–75.
- [3] S.Y. Wang, M.H. Tsai, S.F. Lo, M.J. Tsai, Effects of manufacturing conditions on the adsorption capacity of heavy metal ions by Makino bamboo charcoal, *Bioresour. Technol.* 99 (2008) 7023–7033.
- [4] F.Y. Wang, H. Wang, J.W. Ma, Adsorption of cadmium (II) ions from aqueous solution by a new low-cost adsorbent—Bamboo charcoal, *J. Hazard. Mater.* 177 (2010) 300–306.
- [5] G.Q. Wu, X. Zhang, H. Hui, J. Yan, Q.S. Zhang, J.L. Wan, Y. Dai, Adsorptive removal of aniline from aqueous solution by oxygen plasma irradiated bamboo based activated carbon, *Chem. Eng. J.* 185–186 (2012) 201–210.
- [6] B.H. Hameed, M.I. El-Khaiary, Equilibrium, kinetics and mechanism of malachite green adsorption on activated carbon prepared from bamboo by K_2CO_3 activation and subsequent gasification with CO_2 , *J. Hazard. Mater.* 157 (2008) 344–351.
- [7] U.S.EPA. Health Effects Assessment For 2-chlorophenol and 2,4-dichlorophenol. Environmental Criteria and Assessment Office, Office of Research and Development, Cincinnati, OH, 1986.
- [8] F.W. Shaarani, B.H. Hameed, Ammonia-modified activated carbon for the adsorption of 2,4-dichlorophenol, *Chem. Eng. J.* 169 (2011) 180–185.
- [9] L. Wang, J. Zhang, R. Zhao, C.L. Zhang, C. Li, Y. Li, Adsorption of 2,4-dichlorophenol on Mn-modified activated carbon prepared from *Polygonum orientale* Linn, *Desalination* 266 (2011) 175–181.
- [10] M. Sathishkumar, A.R. Binupriya, D. Kavitha, R. Selvakumar, R. Jayabalan, J.G. Choi, S.E. Yun, Adsorption potential of maize cob carbon for 2,4-dichlorophenol removal from aqueous solutions: Equilibrium, kinetics and thermodynamics modeling, *Chem. Eng. J.* 147 (2009) 265–271.
- [11] K. Eisuke, A. Shoko, N. Takato, Vascular bundle shape in cross-section and relaxation properties of Moso bamboo (*Phyllostachys pubescens*), *Mater. Sci. Eng. C* 31 (2011) 1050–1054.
- [12] H.C. Huang, D.Q. Ye, B.C. Huang, Nitrogen plasma modification of viscose-based activated carbon fibers, *Surf. Coat. Tech.* 201 (2007) 9533–9540.

- [13] L. Ren, J. Zhang, Y. Li, C.L. Zhang, Preparation and evaluation of cattail fiber-based activated carbon for 2,4-dichlorophenol and 2,4,6-trichlorophenol removal, *Chem. Eng. J.* 168 (2011) 553–561.
- [14] F.W. Shaarani, B.H. Hameed, Batch adsorption of 2,4-dichlorophenol onto activated carbon derived from agricultural waste, *Desalination* 255 (2010) 159–164.
- [15] S. Kodama, H. Sekiguchi, Estimation of point of zero charge for activated carbon treated with atmosphere pressure non-thermal oxygen plasma, *Thin. Solid. Films.* 506–507 (2006) 327–330.
- [16] J.P. Wang, Y.X. Chen, H.M. Feng, S.J. Zhang, H.Q. Yu, Removal of 2,4-dichlorophenol from aqueous solution by static-air-activated carbon fibers, *J. Colloid. Interf. Sci.* 313 (2007) 80–85.
- [17] J.P. Wang, H.M. Feng, H.Q. Yu, Analysis of adsorption characteristics of 2,4-dichlorophenol from aqueous solutions by activated carbon fiber, *J. Hazard. Mater.* 144 (2007b) 200–207.
- [18] Z. Alam, S.A. Muyibi, J. Toramae, Statistical optimization of adsorption processes for removal of 2,4-dichlorophenol by activated carbon derived from oil palm empty fruit bunches, *J. Environ. Sci.* 19 (2007) 674–677.
- [19] Y. Zhou, H.F. Jin, Z.L. Chen, Study of adsorption of 2,4-dichlorophenol from aqueous solutions using organic bentonite, *J. Fujian Normal Univ.* 26 (2008) 57–65.
- [20] X.D. Zhu, H.D. Liang, S.L. Zhao, S.Q. Chen, Y. Wang, Y. Shen, The adsorptive characteristics of carbon nanotubes to 2-nitrophenol and 2,4-dichloropheno, *J. Saf. Environ.* 8 (2008) 41–43.
- [21] X.R. Qian, L.J. Wang, R. Shao, A.R. Mao, Preparation of cationic sawdust cellulose and its adsorption to 2,4-dichlorophenol in aqueous solution, *Chin. J. Process Eng.* 9 (2009) 1074–1079.
- [22] R.X. Wang, B.J. Gao, Preparation and 2,4-dichlorophenol Adsorption Behavior of Cross-Linked Polyvinylimidazole Microspheres, *J. Funct. Polym.* 23 (2010) 275–282.